

Ligand Effects on Rates and Regioselectivities of Rh(I)-Catalyzed (5 + 2) Cycloadditions: A Computational Study of Cyclooctadiene and Dinaphthocyclooctatetraene as Ligands

Xiufang Xu,^{†,§} Peng Liu,[§] Adam Lesser,[‡] Lauren E. Sirois,[‡] Paul A. Wender,^{*,‡} and K. N. Houk^{*,§}

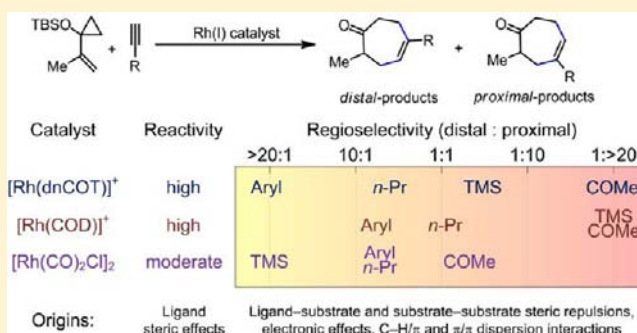
[†]Department of Chemistry, Nankai University, Tianjin, 300071, P.R. China

[§]Department of Chemistry and Biochemistry, University of California, Los Angeles, Los Angeles, California 90095-1569, United States

[‡]Departments of Chemistry and Chemical and Systems Biology, Stanford University, Stanford, California 94305-5080, United States

S Supporting Information

ABSTRACT: The first theoretical study on the effects of ligands on the mechanism, reactivities, and regioselectivities of Rh(I)-catalyzed (5 + 2) cycloadditions of vinylcyclopropanes (VCPs) and alkynes has been performed using density functional theory (DFT) calculations. Highly efficient and selective intermolecular (5 + 2) cycloadditions of VCPs and alkynes have been achieved recently using two novel rhodium catalysts, $[\text{Rh}(\text{dnCOT})]^+\text{SbF}_6^-$ and $[\text{Rh}(\text{COD})]^+\text{SbF}_6^-$, which provide superior reactivities and regioselectivities relative to that of the previously reported $[\text{Rh}(\text{CO})_2\text{Cl}]_2$ catalyst. Computationally, the high reactivities of the dnCOT and COD ligands are attributed to the steric repulsions that destabilize the Rh-product complex, the catalyst resting state in the catalytic cycle. The regioselectivities of reactions with various alkynes and different Rh catalysts are investigated, and a predictive model is provided that describes substrate–substrate and ligand–substrate steric repulsions, electronic effects, and noncovalent π/π and C–H/ π interactions. In the reactions with dnCOT or COD ligands, the first new C–C bond is formed proximal to the bulky substituent on the alkyne to avoid ligand–substrate steric repulsions. This regioselectivity is reversed either by employing the smaller $[\text{Rh}(\text{CO})_2\text{Cl}]_2$ catalyst to diminish the ligand–substrate repulsions or by using aryl alkynes, for which the ligand–substrate interactions become stabilizing due to π/π and C–H/ π dispersion interactions. Electron-withdrawing groups on the alkyne prefer to be proximal to the first new C–C bond to maximize metal–substrate back-bonding interactions. These steric, electronic, and dispersion effects can all be utilized in designing new ligands to provide regiochemical control over product formation with high selectivities. The computational studies reveal the potential of employing the dnCOT family of ligands to achieve unique regiochemical control due to the steric influences and dispersion interactions associated with the rigid aryl substituents on the ligand.



1. INTRODUCTION

Transition metal-catalyzed (5 + 2) cycloadditions of vinylcyclopropanes (VCPs) and 2π -components provide a new reaction for seven-membered ring synthesis and, through variations of participating VCPs, substrates and additives, the conceptual foundation for new routes to five-, six-, eight-, and nine-membered rings.¹ In 1995, Wender's group reported the first examples of intramolecular (5 + 2) cycloaddition of VCPs catalyzed by $[\text{RhCl}(\text{PPh}_3)_3]$.² The intermolecular reactions with alkynes and allenes were described later using $[\text{Rh}(\text{CO})_2\text{Cl}]_2$ as a precatalyst.^{3,4} Since the first reports of the (5 + 2) reaction, a large variety of metal catalysts and ligands have been shown to effect the reaction.^{5,6} Rh-catalysts, such as $[\text{Rh}(\text{dppb})\text{Cl}]_2$,⁷ $[\text{Rh}(\text{naphthalene})(\text{COD})]^+\text{SbF}_6^-$,^{8,9} $[\text{Rh}(\text{NHC})\text{Cl}(\text{COD})]$,¹⁰ and $[\text{Rh}(\text{COD})\text{Cl}]_2$,¹¹ are usually the most efficient among the transition metals, being effective in both inter- and intramolecular reactions. Also reported is a

water-soluble Rh(I) catalyst that effects the (5 + 2) cycloadditions in minimal organic solvent.¹² Asymmetric (5 + 2) cycloadditions have also been achieved using Rh catalysts with chiral bisphosphine¹³ or phosphoramidite¹⁴ ligands. The (5 + 2) cycloaddition has also led to the discovery of new cycloadditions such as (5 + 2 + 1),¹⁵ (5 + 1 + 2 + 1),¹⁶ (3 + 2),¹⁷ and (5 + 1)¹⁸ reactions of VCPs and various π -systems, (5 + 2) and (6 + 2) cycloadditions employing allenylcyclopropanes¹⁹ or vinylcyclobutanones²⁰ as alternative five- or six-carbon synthons.^{21,22}

In contrast to the various catalysts for intramolecular (5 + 2) cycloadditions, the intermolecular reactions have been limited until recently to the use of $[\text{Rh}(\text{CO})_2\text{Cl}]_2$ catalysts. Wender's group reported two novel rhodium(I) catalysts for intermo-

Received: April 30, 2012

Published: June 5, 2012

Table 1. Rh(I)-Catalyzed Intermolecular (5 + 2) Cycloadditions of VCP 1a and Alkynes

| entry | R | catalyst | temp (°C) | time (h) | yield (%) | product ratio ^a | ref. |
|-------|----------------------|---|-----------|----------|-----------|----------------------------|------|
| 1 | TMS 2a | [Rh(dnCOT)(MeCN) ₂] ⁺ SbF ₆ ⁻ | 23 | 1.5 | 92 | 1:4 | 23 |
| 2 | | [(C ₁₀ H ₈)Rh(COD)] ⁺ SbF ₆ ⁻ | 23 | 1.5 | 54 | 1:>20 | 23 |
| 3 | | [Rh(CO) ₂ Cl] ₂ | 40 | 18 | 85 | >20:1 | 3e |
| 4 | <i>n</i> -Pr 2b | [Rh(dnCOT)(MeCN) ₂] ⁺ SbF ₆ ⁻ | 23 | 1 | 74 | 5.4:1 | 23 |
| 5 | | [(C ₁₀ H ₈)Rh(COD)] ⁺ SbF ₆ ⁻ | 23 | 0.75 | 57 | 1.1:1 | 23 |
| 6 | | [Rh(CO) ₂ Cl] ₂ | 40 | 48 | 76 | 7.1:1 | 3e |
| 7 | COMe 2c | [Rh(dnCOT)(MeCN) ₂] ⁺ SbF ₆ ⁻ | 23 | 0.25 | 96 | 1:20 | 23 |
| 8 | | [(C ₁₀ H ₈)Rh(COD)] ⁺ SbF ₆ ⁻ | 23 | 0.25 | 65 | 1:>20 | 23 |
| 9 | | [Rh(CO) ₂ Cl] ₂ | 40 | 2.75 | 91 | 1:1.9 | 3e |
| 10 | Ph 2d | [Rh(dnCOT)(MeCN) ₂] ⁺ SbF ₆ ⁻ | 23 | 1 | 95 | >20:1 | 23 |
| 11 | | [(C ₁₀ H ₈)Rh(COD)] ⁺ SbF ₆ ⁻ | 23 | 0.5 | 68 | 6.8:1 | 23 |
| 12 | | [Rh(CO) ₂ Cl] ₂ | 40 | 7 | 78 | 7.7:1 | 3e |
| 13 | <i>p</i> -OMe-Ph 2e | [Rh(dnCOT)(MeCN) ₂] ⁺ SbF ₆ ⁻ | 23 | 1 | 85 | >20:1 | 23 |
| 14 | | [Rh(CO) ₂ Cl] ₂ | 40 | 5.5 | 76 | 5.9:1 | 3e |
| 15 | <i>p</i> -COMe-Ph 2f | [Rh(dnCOT)(MeCN) ₂] ⁺ SbF ₆ ⁻ | 23 | 1 | 87 | >20:1 | 23 |
| 16 | | [Rh(CO) ₂ Cl] ₂ | 40 | 9 | 66 | 11:1 | 3e |

^aRatio of *distal*-3:*proximal*-3.

lecular (5 + 2) cycloadditions, [(C₁₀H₈)Rh(COD)]⁺SbF₆⁻ and [Rh(dnCOT)(MeCN)₂]⁺SbF₆⁻ (dnCOT = dinaphthocyclooctatetraene, COD = cyclooctadiene, C₁₀H₈ = naphthalene).^{9,23} Both catalysts displayed greater reactivities and regioselectivities than [Rh(CO)₂Cl]₂ in intermolecular (5 + 2) reactions. Cycloadditions using [Rh(CO)₂Cl]₂ often require elevated temperatures and longer reaction times which sometimes allow for competing processes (e.g., alkyne cyclotrimerization). In contrast, both [(C₁₀H₈)Rh(COD)]⁺SbF₆⁻ and [Rh(dnCOT)(MeCN)₂]⁺SbF₆⁻ give superior yields and mode selectivities at room temperature and with shorter reaction times. Good to excellent regioselectivities are often achieved in this process (Table 1). Interestingly, enhanced or even reversed regioselectivities are observed by either altering the ligand or the substrate. For example, the cycloaddition of VCP 1a and TMS acetylene 2a using [Rh(CO)₂Cl]₂ forms the distal product *distal*-3 exclusively (entry 3), while the [(C₁₀H₈)Rh(COD)]⁺SbF₆⁻ catalyst leads exclusively to the proximal product *proximal*-3 (entry 2). Here, we define *proximal* as the alkyne substituent R being positioned nearer to the methyl group of VCP 1a in the product and *distal* as R being positioned further away from the methyl group on VCP 1a in the product. The [Rh(dnCOT)(MeCN)₂]⁺SbF₆⁻ catalyst gives moderate regioselectivity for this reaction, favoring the proximal product (entry 1). In contrast, the [Rh(dnCOT)(MeCN)₂]⁺SbF₆⁻ catalyst gives the highest regioselectivities among the three catalysts in reactions with aryl alkynes 2d–f, leading to the distal products exclusively. Substituents on the alkyne also dramatically affect the regioselectivities. Regardless of the catalyst used, the reaction of VCP 1a with butynone 2c

led to proximal products (entries 7–9), while reactions with alkyl or aryl acetylenes always led to distal products (entries 4–6, 10–16). In these reactions, [Rh(CO)₂Cl]₂ only yields moderate to good regioselectivities, while the [Rh(dnCOT)(MeCN)₂]⁺SbF₆⁻ catalyst enhances the regioselectivities in both cases and leads to complete regiochemical reversals when alkynes 2c or 2d–f are used.

The dramatic effects of ligands on reactivities and regioselectivities necessitate the use of theoretical tools to investigate the origins of these effects as needed to for predictive synthetic applications and for new catalyst design. In our previous theoretical studies we have investigated the mechanism, origins of reactivities, and regioselectivities of [Rh(CO)₂Cl]₂-catalyzed (5 + 2) cycloadditions using density functional theory (DFT) calculations.^{3e,24} In contrast to the experimental discoveries of various catalysts, all theoretical studies to date were performed only with the [Rh(CO)₂Cl]₂ catalyst.²⁵ The origins of the distinct reactivities and regioselectivities of the [Rh(dnCOT)(MeCN)₂]⁺SbF₆⁻ and [(C₁₀H₈)Rh(COD)]⁺SbF₆⁻ catalysts are still unexplored. The differences in performance for these catalysts could be due to changes in mechanism, rate-determining step, or steric/electronic effects of the ligands that alter the energetics of the rate-determining transition states and the catalyst resting states.²⁶ The [Rh(dnCOT)(MeCN)₂]⁺SbF₆⁻ catalyst, based on a relatively little studied COT catalyst ligand,²³ provides much greater regioselectivities than other catalysts in the reactions with aryl acetylenes, which suggests that the naphthyl groups on the dnCOT ligand are essential to achieve high regiochemical control. The differences between cationic and

neutral rhodium catalysts could also play an important role in controlling the reactivities and selectivities. To answer these questions and identify key factors that control reactivities and regioselectivities, we conducted comparative DFT calculations on the intermolecular (5 + 2) cycloadditions of vinylcyclopropanes (VCPs) and a variety of substituted alkynes using three Rh(I) catalysts, $[\text{Rh}(\text{dnCOT})(\text{MeCN})_2]^+\text{SbF}_6^-$, $[(\text{C}_{10}\text{H}_8)\text{Rh}(\text{COD})]^+\text{SbF}_6^-$, and $[\text{Rh}(\text{CO})_2\text{Cl}]_2$. For each catalyst, the mechanisms and origins of reactivities and regioselectivities are investigated and the roles of different ligands are disclosed. Our calculations indicate that the reactivities and regioselectivities are controlled by a combination of steric, electronic effects, and C–H/ π , π/π dispersion interactions. The different effects in these catalysts confer regiochemical control, allowing access to regioisomeric products with high selectivity.

This is also the first computational study on transition metal-catalyzed reactions employing the dnCOT family of ligands. Our computations reveal the strong directing effect of the dnCOT ligand on regioselectivities with aryl-substituted substrates through dispersion interactions with the ligand. These unique features of steric and regiochemical control and the ease of synthesis^{23,27} of dnCOT suggest potentially broader applications of the dnCOT ligand class in a variety of transition metal-catalyzed reactions.

In section 3.1 of this paper, the mechanisms of intermolecular (5 + 2) cycloadditions catalyzed by the two novel catalysts, $[\text{Rh}(\text{dnCOT})(\text{MeCN})_2]^+\text{SbF}_6^-$ and $[(\text{C}_{10}\text{H}_8)\text{Rh}(\text{COD})]^+\text{SbF}_6^-$, are presented and compared with the reaction mechanism involving the $[\text{Rh}(\text{CO})_2\text{Cl}]_2$ catalyst, which has been published previously. The origins of the different reactivities of these catalysts are illustrated. In section 3.2, the origins of regioselectivities in the reactions with various alkynes using these catalysts are analyzed in detail. In section 3.3, the effects of ligands on regioselectivities are summarized.

2. COMPUTATIONAL DETAILS

All geometry optimizations, frequency and solvation energy calculations were performed with the B3LYP²⁸ functional in Gaussian 03.²⁹ The Stuttgart/Dresden effective core potential³⁰ was used on rhodium, and the 6-31G(d) basis set was employed for other atoms. Solvation free energy corrections in 1,2-dichloroethane (DCE) solvent were computed on gas-phase optimized geometries by single point CPCM calculations,³¹ where the United Atom Topological Model (UAHF) was used to define the atomic radii. This is the same methodology that we used in our previous theoretical studies of $[\text{Rh}(\text{CO})_2\text{Cl}]_2$ -catalyzed (5 + 2) cycloadditions.^{3e} Since dispersion interactions were expected to be essential in the regiochemical control in some reactions using $[\text{Rh}(\text{dnCOT})]^+$ and $[\text{Rh}(\text{COD})]^+$ catalysts, Grimme's DFT-D3(BJ) dispersion corrections were calculated using the DFTD3 program.³² We have tested DFT-D3 with original zero-damping³³ and Becke-Johnson finite-damping (DFT-D3(BJ))³⁴ as well as the older version DFT-D2.³⁵ The differences between these different versions were small in our test calculations (see SI for details). Thus, the latest version of DFT-D3 which employs Becke-Johnson finite-damping was used in the calculations. Single point dispersion energy corrections were calculated and added to the B3LYP Gibbs free energies in solution. Figures of three-dimensional molecular structures were prepared using CYLView.³⁶

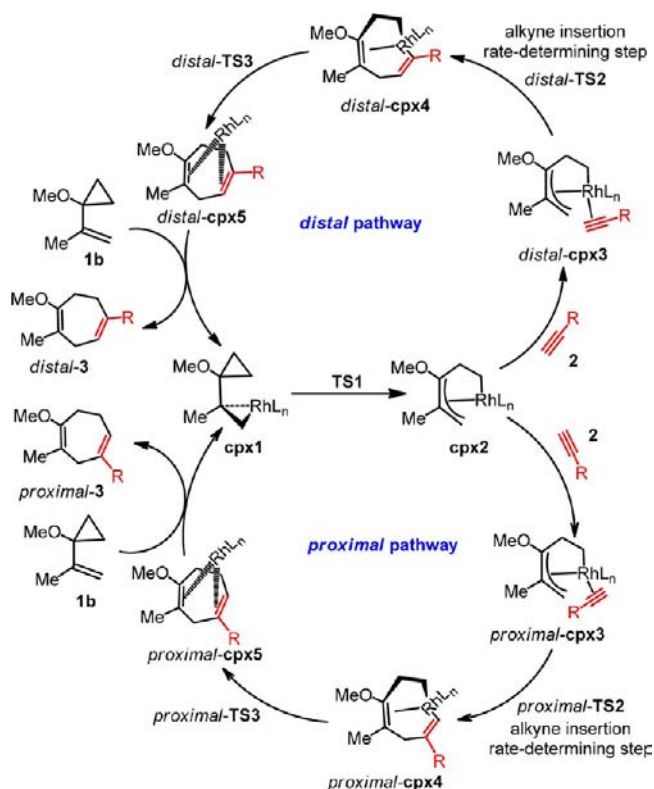
3. RESULTS AND DISCUSSION

3.1. Mechanisms and Origins of Reactivities of $[\text{Rh}(\text{dnCOT})]^+$, $[\text{Rh}(\text{COD})]^+$, and $[\text{Rh}(\text{CO})\text{Cl}]$ -Catalyzed Intermolecular (5 + 2) Cycloadditions. The experimental results indicate that all three Rh(I)-catalysts catalyze the

intermolecular (5 + 2) reactions of VCPs and various alkynes to yield with varying efficiency and selectivity cycloheptenone adducts (see refs 3e, 9, 23, and Table 1). The cationic catalysts, $[\text{Rh}(\text{dnCOT})(\text{MeCN})_2]^+\text{SbF}_6^-$ and $[(\text{C}_{10}\text{H}_8)\text{Rh}(\text{COD})]^+\text{SbF}_6^-$, are much more efficient than $[\text{Rh}(\text{CO})_2\text{Cl}]_2$ and catalyze the reaction at room temperature with good to excellent yields. The reactions with the $[\text{Rh}(\text{CO})_2\text{Cl}]_2$ catalyst also often require elevated temperatures, which in turn promote side reactions such as the cyclotrimerization of alkynes, decomposition of VCP, and formation of secondary isomerization products.^{9a} Moreover, different catalysts lead to significantly different regioselectivities. For example, the $[(\text{C}_{10}\text{H}_8)\text{Rh}(\text{COD})]^+\text{SbF}_6^-$ -catalyzed reaction of VCP **1a** and TMS acetylene **2a** yields *proximal*-product exclusively, but the same reaction using $[\text{Rh}(\text{CO})_2\text{Cl}]_2$ catalyst leads exclusively to *distal*-product (entries 2 and 3 in Table 1). These interesting and contrasting experimental results prompted our analysis of the mechanisms and origins of differences of reactivities and regioselectivities of these reactions and of whether changes of mechanism or rate-determining step are observed with these catalysts.

Our group has previously investigated the mechanisms of $[\text{Rh}(\text{CO})_2\text{Cl}]_2$ -catalyzed intermolecular (5 + 2) cycloadditions using DFT calculations.²⁴ Of the two proposed mechanisms (cyclopropane cleavage first or second), the DFT-preferred mechanism was found to involve initial cyclopropane ring-opening, alkyne insertion, reductive elimination, and ligand exchange to regenerate the Rh-VCP complex (Scheme 1). Alkyne insertion was found to be the rate-determining step in $[\text{Rh}(\text{CO})_2\text{Cl}]_2$ -catalyzed reactions. In reactions with unsymmetrical alkynes, different orientations of the alkyne in the alkyne insertion step led to the distal and proximal

Scheme 1. Catalytic Cycle of Rh(I)-Catalyzed (5 + 2) Cycloaddition of VCP **1b and Alkynes**



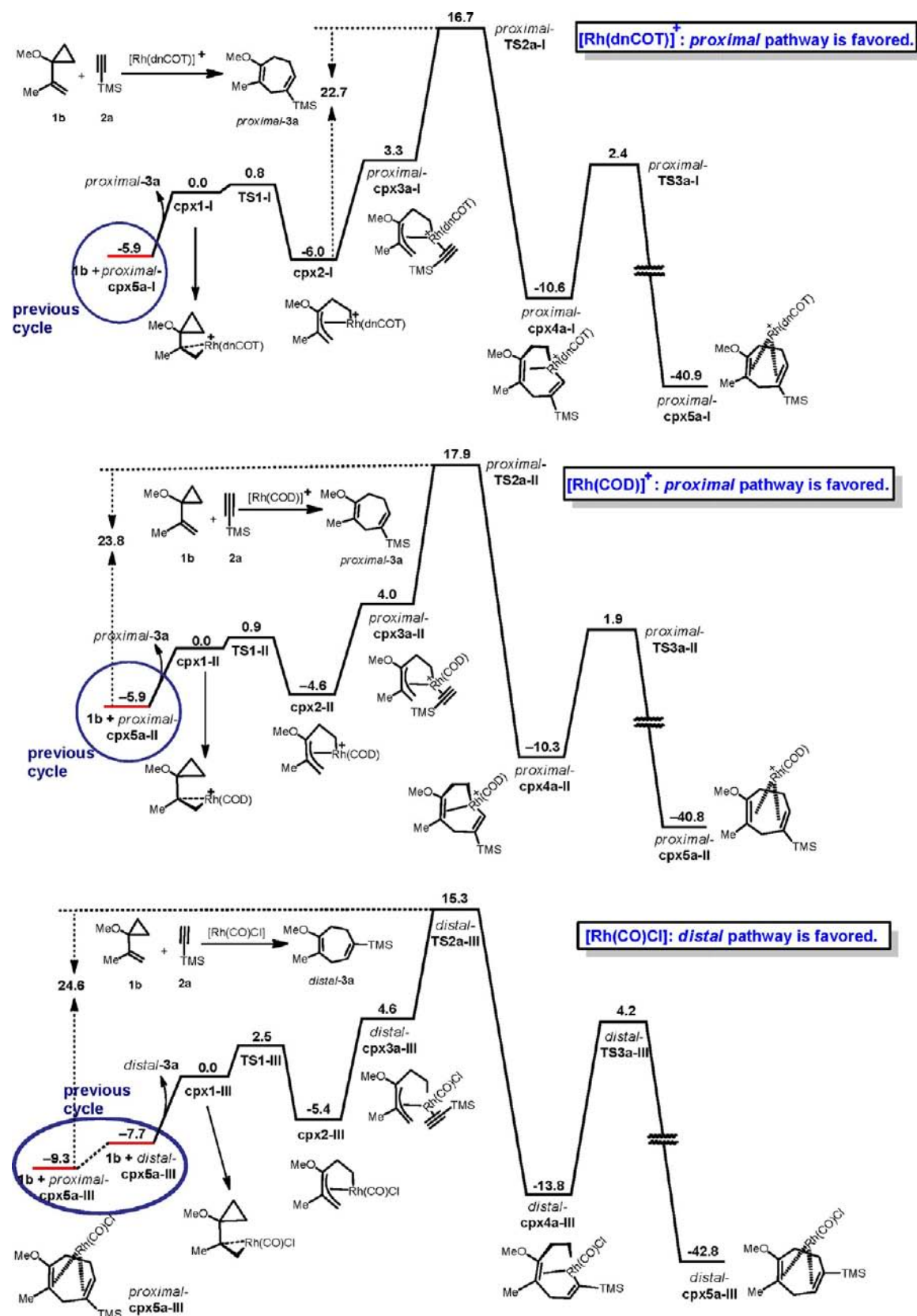


Figure 1. Gibbs free energy surfaces of the favored pathways of intermolecular (5 + 2) cycloadditions of VCP **1b** and TMS acetylene **2a** using [Rh(dnCOT)]⁺, [Rh(COD)]⁺, and [Rh(CO)Cl] catalysts, respectively. Energies are in kcal/mol and calculated using B3LYP/SDD-6-31G(d)/CPCM(DCE).

regioisomeric products, respectively. In this work, we have investigated the mechanisms of [Rh(dnCOT)-

(MeCN)₂]⁺SbF₆⁻, [(C₁₀H₈)Rh(COD)]⁺SbF₆⁻, and [Rh(CO)₂Cl]₂-catalyzed intermolecular (5 + 2) cycloadditions of

Table 2. B3LYP/SDD-6-31G(d)/CPCM(DCE) Free Energy Spans for the Intermolecular (5 + 2) Cycloadditions of VCP 1b and TMS Acetylene^a

| entry | catalyst | R | ligand exchange energy (ΔG_{ex}) ^b | $\Delta G(\text{TS2-cpx1})^{\ddagger c}$ | | free energy span ^d | |
|-------|--------------------------|-----|---|--|-------------------------|-------------------------------|-------------------------|
| | | | | <i>distal</i> pathway | <i>proximal</i> pathway | <i>distal</i> pathway | <i>proximal</i> pathway |
| 1 | [Rh(dnCOT)] ⁺ | TMS | 5.9 | 20.0 | 16.7 | 25.9 | 22.7 |
| 2 | [Rh(COD)] ⁺ | TMS | 5.9 | 22.1 | 17.9 | 28.0 | 23.8 |
| 3 | [Rh(CO)Cl] | TMS | 9.3 | 15.3 | 17.5 | 24.6 | 26.8 |

^aEnergies are in kcal/mol. ^bLigand exchange energy to transform product complex **cpx5a** to liberate product and regenerate the Rh-VCP complex **cpx1**. ^cRelative energy of TS2 with respect to that of **cpx1**. ^dFree energy span is the sum of ligand exchange energy and $\Delta G(\text{TS2-cpx1})^{\ddagger}$. The preferred pathway for each reaction is highlighted in bold.

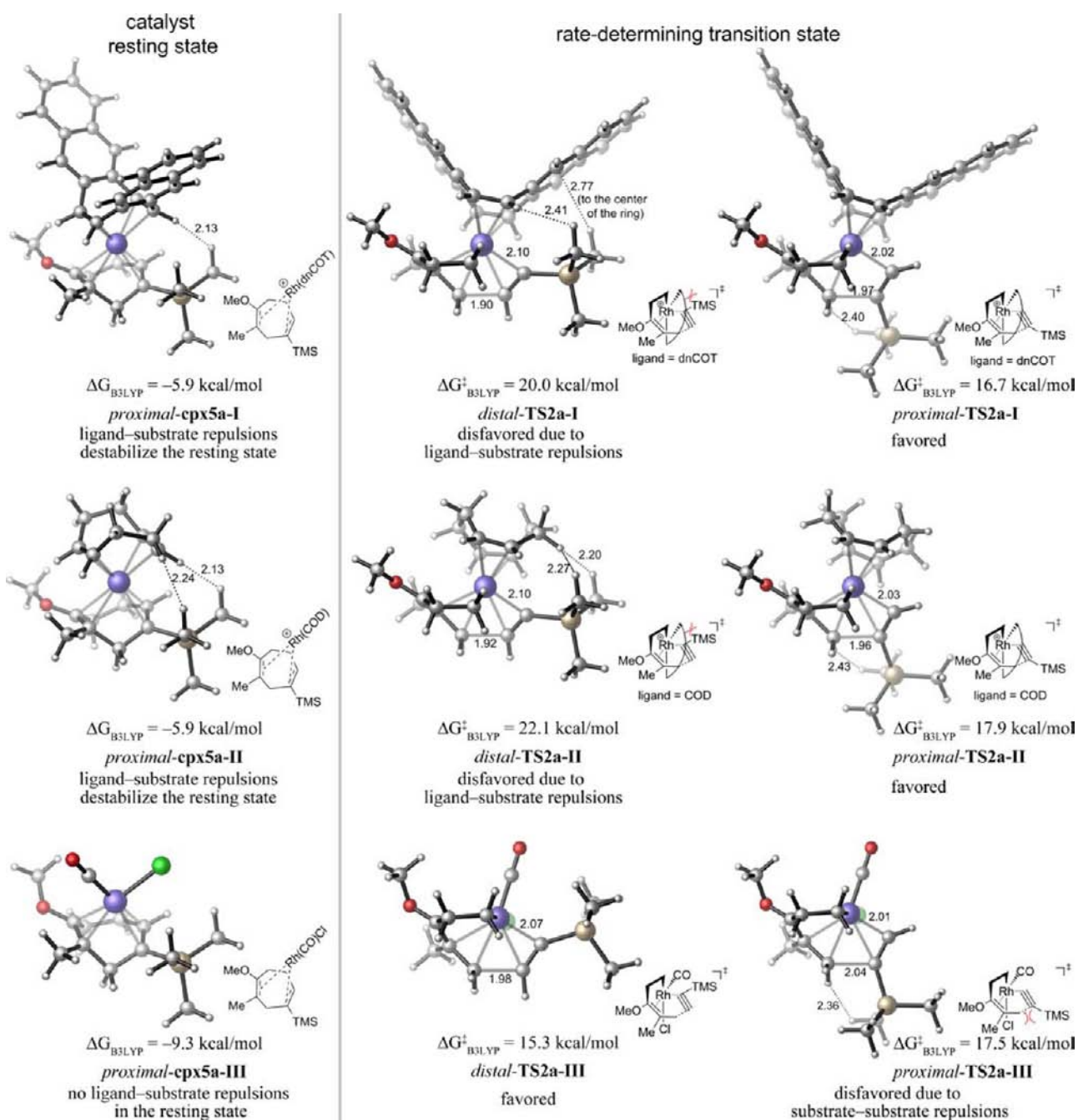


Figure 2. B3LYP/SDD-6-31G(d) optimized geometries of Rh-product complexes *proximal-cpx5a* and alkyne insertion transition states (*distal-* and *proximal-TS2a*) for intermolecular (5 + 2) cycloadditions of VCP 1b and TMS acetylene with three catalysts, [Rh(dnCOT)]⁺, [Rh(COD)]⁺, and [Rh(CO)Cl], respectively. All energies are with respect to the Rh-VCP complex **cpx1**.

VCP with various alkynes using the B3LYP/SDD-6-31G(d) method and the CPCM solvation model. We found that substitution of the alkyne does not affect the mechanism.³⁷ Here we use the reactions of 1-methoxy-1-(prop-1-en-2-yl)cyclopropane VCP **1b** with TMS acetylene **2a** as an example for the discussions of reaction mechanisms and origins of the different reactivities of different catalysts.

We have tested the effects of substituents on the C-1 position of VCP. The $[\text{Rh}(\text{dnCOT})(\text{MeCN})_2]^+\text{SbF}_6^-$ -catalyzed reactions of TMS acetylene **2a** and two VCPs with either OTMS or OMe groups at the C-1 position were calculated. The reactions with the two VCPs gave very similar overall activation barriers and regioselectivities.³⁷ Thus, the OMe substituted VCP **1b** was employed in the calculations to reduce computational time.

In $[\text{Rh}(\text{dnCOT})(\text{MeCN})_2]^+\text{SbF}_6^-$ and $[(\text{C}_{10}\text{H}_8)\text{Rh}(\text{COD})]^+\text{SbF}_6^-$ -catalyzed (5 + 2) reactions, the counterion, SbF_6^- , is thought to act as a spectator during the catalytic process³⁸ and hence is not included in the computations. Before entering the catalytic cycle, two coordination sites in the coordinatively saturated $[\text{Rh}(\text{dnCOT})(\text{MeCN})_2]^+$ and $[(\text{C}_{10}\text{H}_8)\text{Rh}(\text{COD})]^+$ catalysts become occupied by substrates. We have calculated the ligand dissociation energies for these catalysts and found the dissociation of two MeCN molecules from $[\text{Rh}(\text{dnCOT})(\text{MeCN})_2]^+$ is less costly than the dissociation of dnCOT by 26.6 kcal/mol in terms of free energies. Similarly, dissociation of the COD ligand requires 34.4 kcal/mol more energy than that of the weakly bound naphthyl ligand of the $[(\text{C}_{10}\text{H}_8)\text{Rh}(\text{COD})]^+$ catalyst. This suggests that the Rh binds to dnCOT and COD instead of MeCN or C_{10}H_8 in the catalytic cycle. This agrees with the experimental observations that reactions in MeCN solvent proceed very slowly, presumably due to unfavorable ligand dissociation to form the active catalyst. An active catalytic species for intermolecular (5 + 2) cycloadditions can also be generated in situ from $[\text{Rh}(\text{COD})\text{Cl}]_2$ and AgSbF_6 , which leads to similar reactivity as the $[(\text{C}_{10}\text{H}_8)\text{Rh}(\text{COD})]^+\text{SbF}_6^-$ catalyst.^{9a} This result again suggests that Rh binds to COD instead of C_{10}H_8 in the catalytic cycle. In our previous theoretical studies, the dimeric precatalyst, $[\text{Rh}(\text{CO})_2\text{Cl}]_2$, was found to dissociate and eliminate one CO to form the active catalyst, $[\text{Rh}(\text{CO})\text{Cl}]$, before it enters the catalytic cycle.^{24a} Therefore, the active catalysts used in the current computations are $[\text{Rh}(\text{dnCOT})]^+$, $[\text{Rh}(\text{COD})]^+$, and $[\text{Rh}(\text{CO})\text{Cl}]$, respectively.

Both the *distal* and *proximal* pathways in $[\text{Rh}(\text{dnCOT})]^+$, $[\text{Rh}(\text{COD})]^+$, and $[\text{Rh}(\text{CO})\text{Cl}]$ -catalyzed cycloaddition of VCP **1b** and TMS acetylene **2a** were calculated and the Gibbs free energy surfaces of the preferred pathways are shown in Figure 1. Our calculations indicated that altering the catalyst does not change the mechanism or the rate-determining step, but does change preferences for the *distal* or *proximal* pathways. Reactions with all catalysts proceed via the mechanism as depicted in Scheme 1.³⁹ The rate-determining step is the alkyne insertion (**TS2a**) to form the eight-membered metallacycle intermediates. The activation barriers for cyclopropane ring-opening (**TS1a**) and reductive elimination (**TS3a**) are both much lower than alkyne insertion. The catalyst resting state in the catalytic cycle is the Rh-product π complex (**cpx5a**).⁴⁰ Thus, the free energy spans, i.e. the overall barriers, for these reactions are calculated by the energy difference between **TS2a** and the product complex **cpx5a** in the previous cycle.^{41,42} This can be calculated by the sum of the ligand exchange energy (ΔG_{ex}) of the Rh-product complex **cpx5a** to liberate the

product and regenerate the Rh-VCP complex **cpx1** and the energy of **TS2a** with respect to **cpx1** ($\Delta G(\text{TS2-cpx1})^\ddagger$).

The free energy spans of both distal and proximal pathways with the three catalysts are summarized in Table 2. Since the mechanism and reactivity are determined by the lowest energy pathway, we limit the discussion in this section to the preferred pathway with each catalyst (marked in bold in Table 2). Detailed implications of the divergent regioisomeric pathways are addressed in section 3.2. In reactions with $[\text{Rh}(\text{dnCOT})]^+$ and $[\text{Rh}(\text{COD})]^+$ catalysts, the proximal pathway is preferred. The free energy span is 22.7 and 23.8 kcal/mol, respectively. The reaction with $[\text{Rh}(\text{CO})\text{Cl}]$ prefers the distal pathway, with a higher free energy span of 24.6 kcal/mol, in agreement with its lower reactivity in experiment. The higher free energy span with $[\text{Rh}(\text{CO})\text{Cl}]$ mainly arises from the ligand exchange energy (ΔG_{ex}), the energy to liberate the product from the Rh-product complex (**cpx5a**) and form the Rh-VCP complex (**cpx1**). Two regioisomeric product complexes are possible for each reaction: *distal-cpx5a* and *proximal-cpx5a*. The proximal product complexes are slightly more stable than the distal complexes, and are used to calculate the ligand exchange energies and the overall activation barriers.⁴³ The ligand exchange with bulkier dnCOT and COD ligands both require 5.9 kcal/mol. For the reaction with $[\text{Rh}(\text{CO})\text{Cl}]$, much higher ligand exchange energy is required ($\Delta G_{\text{ex}} = 9.3$ kcal/mol). The smaller ligand exchange energies with bulkier ligands are due to the destabilizing steric repulsions in the Rh-product complexes between the ligand and the cycloheptadiene product, especially with the TMS group. The shortest H–H distances between the ligand and the product in the Rh-product complexes, *proximal-cpx5a-I* and *proximal-cpx5a-II*, are both only 2.13 Å (Figure 2). The ligand-product steric repulsions destabilize the Rh-product complexes with the bulky dnCOT and COD ligands, and lead to lower ligand exchange energies and higher reactivities.

The other component in the overall free energy span is the relative energy of the alkyne insertion transition state (**TS2**) with respect to the Rh-VCP complex **cpx1** ($\Delta G(\text{TS2-cpx1})^\ddagger$). The *distal* pathway is preferred with the $[\text{Rh}(\text{CO})\text{Cl}]$ catalyst ($\Delta G(\text{TS2-cpx1})^\ddagger = 15.3$ kcal/mol), while the distal transition states with bulkier dnCOT and COD ligands are disfavored due to ligand-substrate repulsions. In the proximal pathway, the TMS group is oriented away from the ligand with minimal steric interactions with the ligand. Thus, the computed energies of the three proximal transition states are similar. These proximal transition states are 1–2 kcal/mol less stable than the preferred distal transition state with $[\text{Rh}(\text{CO})\text{Cl}]$.

In summary, bulkier ligands destabilize the catalyst resting state, the Rh-product complex *proximal-cpx5a*, while having minimal effects on the *proximal* alkyne insertion transition state (*proximal-TS2*). Thus, these bulky ligands promote the proximal pathway, and, more significantly, lead to increased reactivity. The overall activation barriers for reactions with COD and dnCOT ligands are 0.8 and 1.9 kcal/mol lower than for the reaction with $[\text{Rh}(\text{CO})\text{Cl}]$. This corresponds to 10–100 times faster reactions, in agreement with experiments.

3.2. Origins of Regioselectivities. **3.2.1. Regioselectivities Predicted by B3LYP and B3LYP-D3(BJ) Calculations: Comparison of Methods.** Besides the effects on reactivities discussed above, ligands also play a key role in determining the regioselectivities of the cycloaddition products. When unsymmetrical alkynes are used in the intermolecular (5 + 2) cycloadditions, two regioisomeric products could be formed (Scheme 1). As discussed in the introduction, the three

Table 3. B3LYP/SDD-6-31G(d)/CPCM(DCE) and D3(BJ)-Corrected Regioselectivities for (5 + 2) Cycloadditions of VCP **1b** and Substituted Alkynes

| entry | R | catalyst | B3LYP/SDD-6-31G(d)/CPCM(DCE) | | B3LYP-D3(BJ)/SDD-6-31G(d)/CPCM(DCE) | | exp. ratio ^b |
|-------|-----------------------------|--------------------------|--|------------------------------|--|------------------------------|-------------------------|
| | | | $\Delta\Delta G^\ddagger$ (dist-prox) ^a | predicted ratio ^b | $\Delta\Delta G^\ddagger$ (dist-prox) ^a | predicted ratio ^b | |
| 1 | TMS 2a | [Rh(dnCOT)] ⁺ | 3.2 | 1:>20 | -0.6 | 2.8:1 | 1:4 |
| 2 | | [Rh(COD)] ⁺ | 4.2 | 1:>20 | 2.8 | 1:>20 | 1:>20 |
| 3 | | [Rh(CO)Cl] | -2.0 | >20:1 | -2.8 | >20:1 | >20:1 |
| 4 | <i>n</i> -Pr 2b | [Rh(dnCOT)] ⁺ | -0.1 | 1.2:1 | -2.3 | >20:1 | 5.4:1 |
| 5 | | [Rh(COD)] ⁺ | -0.1 | 1.2:1 | -1.7 | 17.6:1 | 1.1:1 |
| 6 | | [Rh(CO)Cl] | -1.2 | 7.6:1 | -1.4 | 10.6:1 | 7.1:1 |
| 7 | COMe 2c | [Rh(dnCOT)] ⁺ | 4.3 | 1:>20 | 1.9 | 1:>20 | 1:20 |
| 8 | | [Rh(COD)] ⁺ | 1.8 | 1:>20 | 0.3 | 1:1.8 | 1:>20 |
| 9 | | [Rh(CO)Cl] | 1.6 | 1:14.9 | 1.0 | 1:5.4 | 1:1.9 |
| 10 | NH ₂ 2g | [Rh(dnCOT)] ⁺ | -3.9 | >20:1 | -5.9 | >20:1 | N/A |
| 11 | | [Rh(COD)] ⁺ | -1.8 | >20:1 | -2.5 | >20:1 | N/A |
| 12 | | [Rh(CO)Cl] | -3.6 | >20:1 | -4.0 | >20:1 | N/A |
| 13 | Ph 2d | [Rh(dnCOT)] ⁺ | 1.4 | 1:10.6 | -3.4 | >20:1 | >20:1 |
| 14 | | [Rh(COD)] ⁺ | 0.9 | 1:4.6 | -1.4 | 10.6:1 | 6.8:1 |
| 15 | | [Rh(CO)Cl] | -2.1 | >20:1 | -2.8 | >20:1 | 7.7:1 |
| 16 | <i>p</i> -OMe-Ph 2e | [Rh(dnCOT)] ⁺ | 1.5 | 1:12.6 | -3.6 | >20:1 | >20:1 |
| 17 | | [Rh(CO)Cl] | -1.8 | >20:1 | -2.5 | >20:1 | 5.9:1 |
| 18 | <i>p</i> -COMe-Ph 2f | [Rh(dnCOT)] ⁺ | 1.0 | 1:5.4 | -4.4 | >20:1 | >20:1 |
| 19 | | [Rh(CO)Cl] | -2.4 | >20:1 | -3.0 | >20:1 | 11:1 |

^aGibbs free energy differences between *distal*-TS2 and *proximal*-TS2 in kcal/mol. ^bRatio of *distal*-3: *proximal*-3.

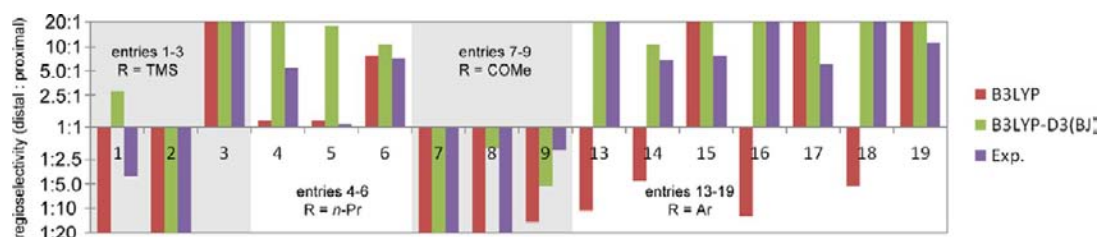


Figure 3. Comparison of B3LYP and B3LYP-D3(BJ) predicted regioselectivities with experimental product ratios. Logarithmic scale was used for the y axis (regioselectivity).

different catalysts exhibit distinct regiochemical control in reactions with various alkynes. Reversals of regioselectivities are observed by either altering the catalyst or the substituent on the alkyne (Table 1).

DFT investigations of the catalytic cycles (see previous section) suggest that the rate- and regioselectivity-determining step is the alkyne insertion for reactions with all three catalysts investigated. The relative energies of the distal and proximal alkyne insertion transition states (TS2) determine the regioselectivity, which could be controlled by steric and electronic effects as well as by dispersion interactions between the substrates and the ligand, such as π/π and C-H/ π interactions. We performed density functional theory calcu-

lations to investigate the origins of regioselectivities in the (5 + 2) reactions with these different catalysts.

In our previous theoretical studies of the [Rh(CO)Cl]-catalyzed reactions, we found that B3LYP/SDD-6-31G(d) and the CPCM solvation model provide reliable predictions of regioselectivities that are in good agreement with experiment.^{3c} We used the same level of theory in this study to calculate the regioselectivities in reactions with the [Rh(dnCOT)]⁺ and [Rh(COD)]⁺ catalysts. The predicted Gibbs free energy differences between the distal and proximal alkyne insertion transition states and the product ratios are listed in Table 3. These predicted ratios are compared with the experimental results in Figure 3.

B3LYP provided reasonable agreement with the experimental results for all reactions except those with aryl acetylenes. For alkynes without aryl groups (entries 1–9), B3LYP always predicted correct regioisomeric products and reproduced the general trends of regioselectivities. For example, the reactions with 1-pentyne (entries 4–6) give moderate regioselectivities of the distal major products, and the reactions with butynone (entries 7–9) lead to reversed regioselectivities that favor proximal products. For [Rh(CO)Cl]-catalyzed reactions with aryl acetylenes (entries 15, 17, and 19), B3LYP also predicted the correct major products, while the regioselectivities were slightly overestimated. However, B3LYP predicted the wrong major products for [Rh(dnCOT)]⁺- and [Rh(COD)]⁺-catalyzed reactions with aryl acetylenes (entries 13, 14, 16, and 18). We speculated that the poor performance of B3LYP in these systems is due to the improper treatment of noncovalent dispersion interactions by B3LYP. Conventional DFT methods, including B3LYP, are known to significantly underestimate π/π and C–H/ π dispersion energies.⁴⁴ Recently, a number of new density functionals and theoretical dispersion corrections to DFT energetics have been developed to improve the accuracy in treating noncovalent interactions.⁴⁵ In this work, we use Grimme's most recent dispersion correction method, DFT-D3(BJ), to account for the dispersion energies in these systems.³⁴ DFT-D3 provides accurate dispersion corrections to the DFT-computed energies with a minimum of empiricism and is applicable to systems with metal atoms.³³ The most recent variant with BJ-damping (DFT-D3(BJ)) has been reported to perform slightly better than the standard "zero-damping" DFT-D3.³⁴

For all reactions with the [Rh(CO)Cl] catalyst, B3LYP with or without D3(BJ) corrections predicted very similar regioselectivities, always within 1 kcal/mol between these two methods. This suggests that dispersion effects on the regioselectivities in [Rh(CO)Cl]-catalyzed reactions are not significant. This is reasonable since the dispersion interactions between the substrates and the small ligands (CO and Cl) are expected to be small. In contrast, for [Rh(dnCOT)]⁺ and [Rh(COD)]⁺-catalyzed reactions, D3(BJ) provided much larger corrections to the regioselectivities, leading to greater preferences for the distal pathway in all cases. In the distal pathway, the substituent on the alkyne is adjacent to the ligand and greater stabilizing dispersion interactions are expected. The degree of correction by D3(BJ) parallels the size of the alkyne substituent. For smaller alkyne substituents, such as *n*-Pr, COMe, and NH₂, D3(BJ) corrected energies lead to ~2 kcal/mol and 1–1.5 kcal/mol greater preference for the distal pathway for [Rh(dnCOT)]⁺- and [Rh(COD)]⁺-catalyzed reactions, respectively (entries 4, 7, 10, and 5, 8, 11, respectively). For reactions involving TMS and especially aryl substituents, the D3(BJ) corrections are greater and give better agreement with the experimental regioselectivities. For example, the distal pathway in the reactions with phenyl acetylene using [Rh(dnCOT)]⁺ and [Rh(COD)]⁺ catalysts is predicted to be more favorable by B3LYP-D3(BJ) (entries 13 and 14, Table 3). The B3LYP-D3(BJ) predicted regioselectivities, >20: 1 and 10.6: 1, both agree well with the experiment (>20: 1 and 6.8: 1, respectively), while B3LYP energies predicted the wrong major products for both reactions. More details of the effects of dispersion interactions are discussed in section 3.2.2.

It is noted that although the B3LYP-D3(BJ) method gave significant improvements to predicted regioselectivities where

strong dispersion interactions are observed, the D3(BJ) corrections tend to overestimate such corrections and thus lead to greater preference to the distal pathway. This sometimes gives erroneous regioselectivities after the corrections, e.g. for reactions with 1-pentyne (*R* = *n*-Pr, entries 4–6, Table 3), where B3LYP predicts regioselectivities better than the B3LYP-D3(BJ) results.

We also tested the performance of the M06 functional, which is known to provide more accurate dispersion energies than B3LYP.⁴⁶ Similar to B3LYP-D3(BJ), M06 calculations provide much better agreement with the experimental regioselectivities than B3LYP for systems with strong dispersion interactions (see Supporting Information for details). The TS geometries optimized by M06 are also noticeably different from B3LYP-optimized geometries. With more accurate treatment of dispersion interactions, M06 give shorter C–H/ π and π/π distances between the ligand and the substrate. In the cases we tested without strong ligand–substrate dispersion interactions, M06 gives similar results as B3LYP and B3LYP-D3(BJ).

In summary, regioselectivities calculated at the B3LYP/SDD-6-31G(d)/CPCM(DCE) level show good agreement with the experiment for reactions without strong ligand–substrate dispersion interactions. For reactions involving bulky, especially aromatic ligands and alkyne substituents, ligand–substrate dispersion interactions are essential to the regiochemical control. In these cases, B3LYP-D3(BJ) significantly improves the accuracy of predicted regioselectivities.

3.2.2. Regioselectivities in the (5 + 2) Cycloadditions with Different Alkynes. Both theoretical predictions and experiment suggest that there is not a simple trend of regioselectivity in these (5 + 2) cycloadditions. This is not surprising due to the number of reaction and reactant variables and their potentially opposing impacts on the outcome. Especially, reversal of regioselectivities could be achieved by using different alkyne substrates or simply different catalysts. In fact, the regioselectivities are controlled by a mix of steric effects, electronic effects, and dispersion interactions between the substrates and the ligand. We examine the origins of regioselectivities in the reactions with different alkynes in this section and the factors that control regioselectivities are summarized in section 3.3.

3.2.2.1. Reactions with TMS Acetylene: Ligand Steric Effects Reverse Regioselectivity. The reactions of VCP **1b** and TMS acetylene **2a** lead to very different regioselectivities when different ligands are employed (entries 1–3, Table 3). We have previously shown that for reactions with the small [Rh(CO)Cl] catalyst, the repulsions around the forming C–C bond are greater than the repulsions between the alkyne substituent and the ligand.^{3e} Bulkier alkyne substituents, such as TMS, leads to exclusive formation of the distal products. When larger ligands (dnCOT and COD) are employed, the regioselectivities are reversed. Both B3LYP and B3LYP-D3(BJ) predicted that the reaction with the COD ligand leads to exclusive formation of the proximal products. This is in good agreement with the experiment (entry 2). The transition state structures with the COD ligand (*distal-TS2a-II* and *proximal-TS2a-II*) are shown in Figure 2. Both double bonds on COD are bound to the rhodium and are positioned in the same orientation as the CO and Cl groups in the [Rh(CO)Cl] catalyst, i.e. *trans* to the alkyl carbon and the terminal allyl carbon in the Rh-allyl complex, respectively. This conformation points the two –CH₂CH₂– groups on the COD ligand toward the C-1 substituent on the VCP and the substituent on the alkyne. Thus, significant repulsions between the TMS on the alkyne and the CH₂ on the

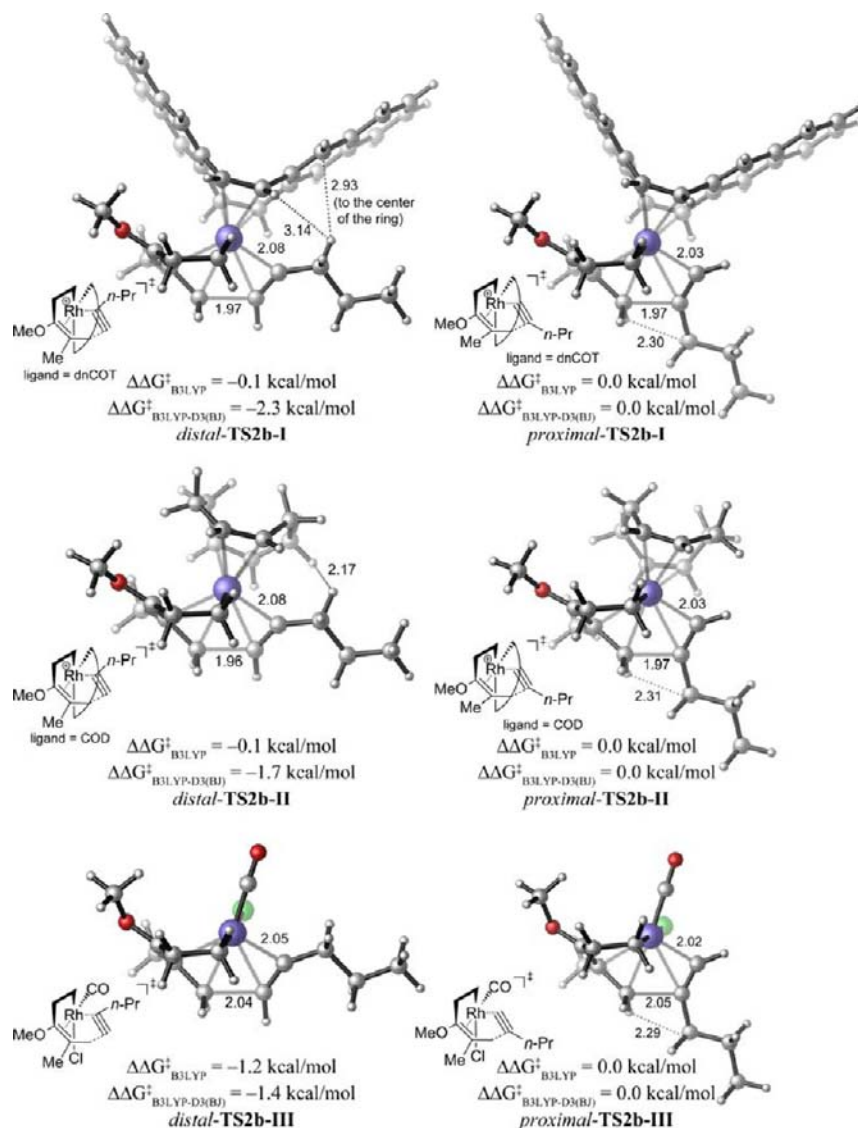


Figure 4. B3LYP/SDD-6-31G(d) optimized geometries of the alkyne insertion transition states for intermolecular (5 + 2) cycloadditions of VCP **1b** and 1-pentyne **2b** with three catalysts: $[\text{Rh}(\text{dnCOT})]^+$, $[\text{Rh}(\text{COD})]^+$, and $[\text{Rh}(\text{CO})\text{Cl}]$, respectively.

ligand are observed in the distal alkyne insertion transition state (*distal-TS2a-II*); the shortest H–H distance is only 2.20 Å. In contrast, no steric interactions between the TMS group and the ligand are observed in the $[\text{Rh}(\text{CO})\text{Cl}]$ -catalyzed transition state. The ligand–substrate repulsions with the bulky COD ligands lead to much higher activation barriers in the distal pathway than the reaction with the smaller $[\text{Rh}(\text{CO})\text{Cl}]$ catalyst. The orientation of the dnCOT ligand in the alkyne insertion transition state is similar to that of the COD ligand: one of the naphthyl groups on the dnCOT ligand points toward the substituent on the alkyne. Both B3LYP and B3LYP-D3(BJ) predicted the proximal pathway is less favorable than with the COD ligand. However, B3LYP overestimated the regioselectivities (1:>20 vs 1:4 in the experiment), presumably due to the poor treatment of B3LYP in predicting dispersion interactions in the distal pathway. In *distal-TS2a-I*, one hydrogen atom on TMS and the naphthyl group on the ligand are positioned to be able to have stabilizing C–H/ π interactions (see Figure 2). B3LYP-D3(BJ) corrects the dispersion energies, but the correction is overestimated. The experimental ratio of 1:4 corresponds to a distal/proximal

energy difference of 0.8 kcal/mol. The D3(BJ) corrected energy difference (–0.6 kcal/mol) deviates from the experiment by 1.4 kcal/mol and the wrong major regioisomer is predicted by B3LYP-D3(BJ).

In summary, the regioselectivity of the (5 + 2) cycloaddition with TMS acetylene is controlled by the steric properties of the ligand. The small $[\text{Rh}(\text{CO})\text{Cl}]$ catalyst leads to exclusive formation of the distal product and the bulky COD ligand leads to exclusive formation of the proximal product. The bulky dnCOT ligand also favors the proximal product, but the regioselectivity is diminished by the stabilizing C–H/ π interactions in the distal pathway.

3.2.2.2. Reactions with 1-Pentyne: Weak Steric Interactions Lead to Moderate Regioselectivity. The distal product is favored in the reaction of VCP **1b** and 1-pentyne **2b** irrespective of the ligand used (entries 4–6, Table 3). The regioselectivities are lower than the reactions with TMS acetylene, which is obviously due to the diminished steric control of the smaller *n*-Pr substituent (Figure 4). The degree of preference for the distal product parallels the trend in the TMS acetylene reactions: $[\text{Rh}(\text{CO})\text{Cl}]$ leads to the highest

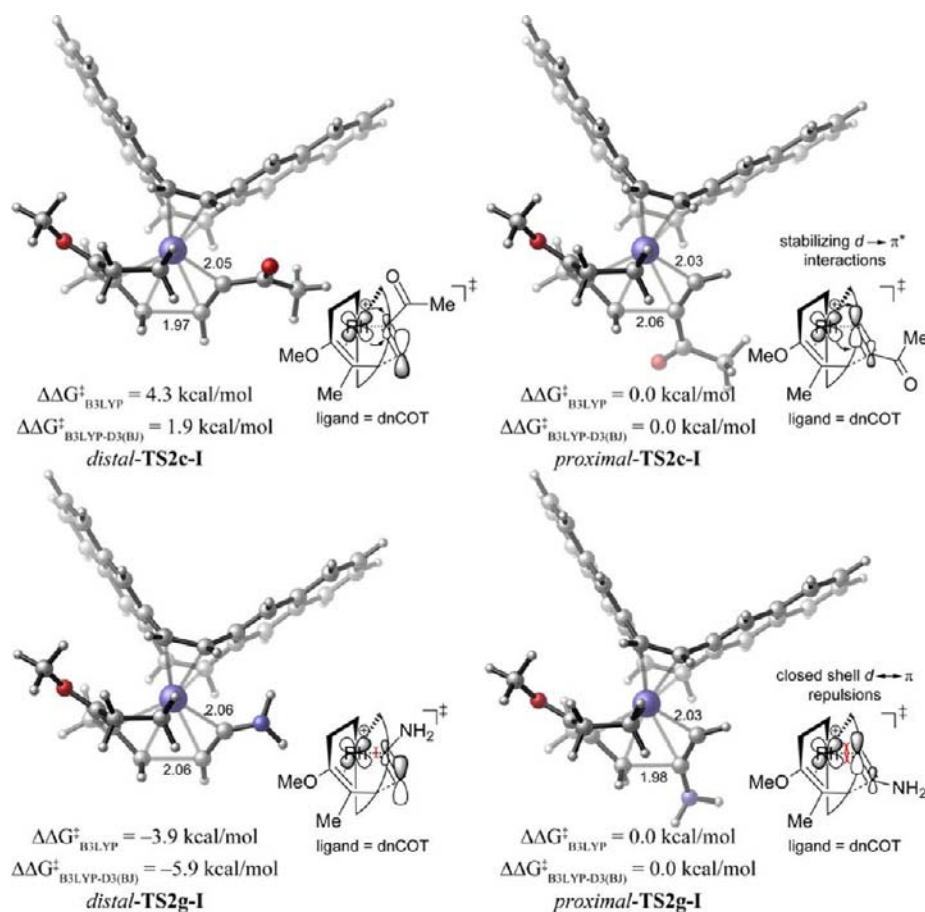


Figure 5. B3LYP/SDD-6-31G(d) optimized geometries of the alkyne insertion transition states for $[\text{Rh}(\text{dnCOT})]^+$ -catalyzed (5 + 2) cycloadditions of VCP **1b** with butynone **2c** and ethynamine **2g**.

selectivity of distal product and $[\text{Rh}(\text{COD})]^+$ leads to the lowest selectivity. The B3LYP results provide good agreement with the experimental selectivities, while the D3(BJ) dispersion corrections overestimate the stabilizing interactions in the distal pathway and thus predict greater regioselectivities than the experiment.

3.2.2.3. Reactions with But-3-yn-2-one and Ethynamine: Combination of Steric and Electronic Effects. Electron-withdrawing groups on the alkyne stabilize the *proximal* alkyne insertion transition state (*proximal-TS2*). This orientation maximizes the overlap between the alkyne out-of-plane π^* orbital and the Rh d orbital, and thus enhances the stabilizing $d \rightarrow \pi^*$ back-donation (Figure 5). In the $[\text{Rh}(\text{CO})\text{Cl}]$ -catalyzed reaction of VCP **1b** and but-3-yn-2-one (**2c**, R = COMe), the strong electronic effects of the COMe group reverse the steric control of regioselectivity and the proximal product is favored. Both B3LYP and B3LYP-D3(BJ) predicted the correct major regioisomer for the $[\text{Rh}(\text{CO})\text{Cl}]$ -catalyzed reaction (entry 9), and B3LYP-D3(BJ) gives better agreement with the experiment than B3LYP.

In the reactions with $[\text{Rh}(\text{dnCOT})]^+$ and $[\text{Rh}(\text{COD})]^+$ catalysts, electronic effects of the electron-withdrawing COMe group also strongly prefer the proximal pathway, and the steric effects are expected to be weak as in the reactions with the similar-sized 1-pentyne. As a result, a combination of these effects leads to exclusive formation of the proximal products in both reactions. B3LYP provided good agreement with the experimental regioselectivities, while B3LYP-D3(BJ) again

overestimates the dispersion corrections for the reaction with $[\text{Rh}(\text{COD})]^+$ and predicts much lower regioselectivity.

In contrast, strongly electron-donating groups are predicted to destabilize *proximal-TS2*. Unlike electron-withdrawing substituents, which mainly polarize the alkyne π^* orbital (LUMO), electron-donating substituents mainly polarize the filled alkyne π orbital (see Supporting Information for more details). Thus, the closed-shell repulsion between the alkyne π orbital and the filled Rh d orbital is more significant in the proximal TS with electron-rich alkynes (Figure 5). In the reactions with ethynamine (**2g**, R = NH_2), the regioselectivity is controlled by electronic effects in reactions with all three catalysts. All reactions are predicted to lead to exclusive formation of the distal product (entries 10–12 in Table 3).⁴⁷

3.2.2.4. Reactions with Aryl Acetylenes: π/π and C-H/ π Interactions Dominate over Steric Effects. In transition metal-catalyzed C–C bond forming reactions with terminal aryl alkynes, the new C–C bond is usually formed at the terminal position to avoid steric repulsions with the aryl group.²⁶ In $[\text{Rh}(\text{CO})\text{Cl}]$ -catalyzed (5 + 2) cycloadditions with terminal aryl alkynes, the distal products are favored, with a similar degree of regiocontrol as the *n*-Pr substituent (Table 3, entries 15, 17, and 19, also see ref 3e). This is attributed to the greater substrate–substrate steric repulsions between the aryl substituents and the VCP in the proximal pathway than the ligand–substrate repulsions in the distal pathway. Experimentally, $[\text{Rh}(\text{dnCOT})]^+$ and $[\text{Rh}(\text{COD})]^+$ catalysts also lead to the distal products in reactions with aryl acetylenes (entries 13, 14, 16, 18). In the $[\text{Rh}(\text{COD})]^+$ -catalyzed reactions, the

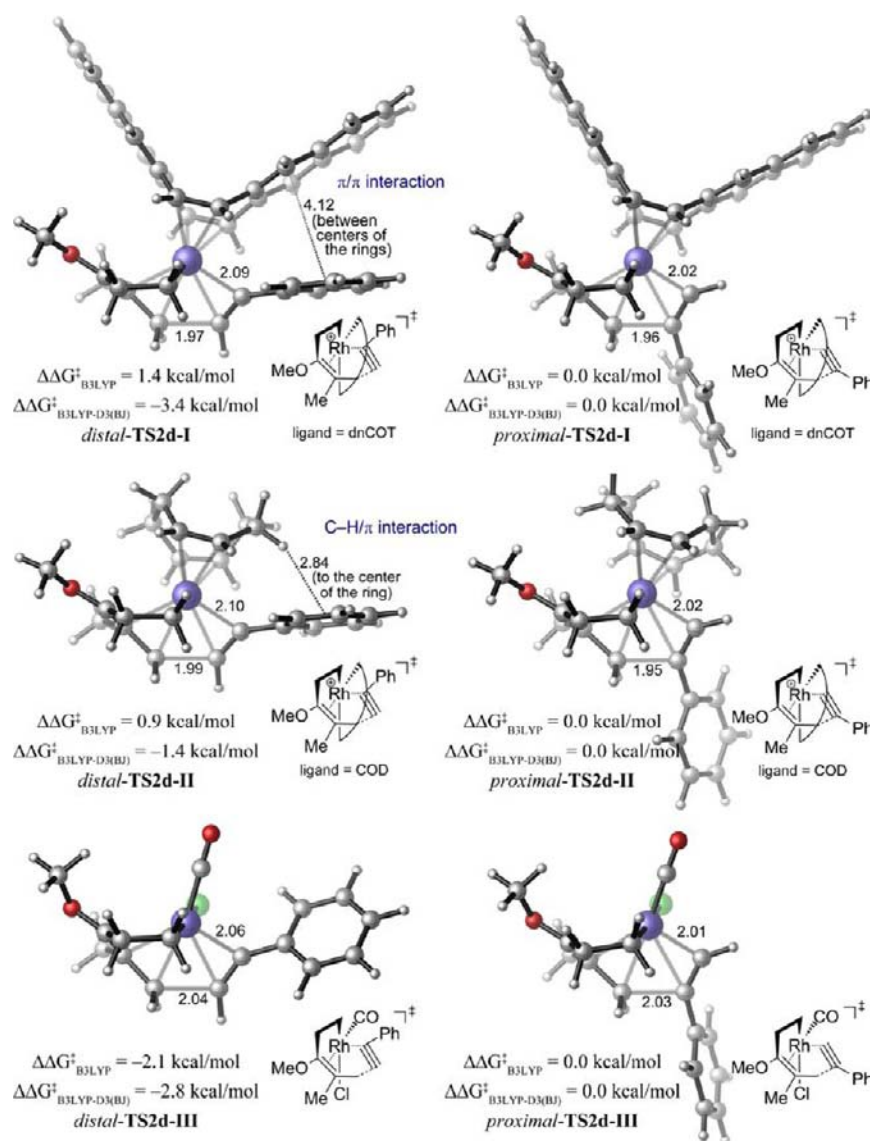


Figure 6. B3LYP/SDD-6-31G(d) optimized geometries of the alkyne insertion transition states for [Rh(dnCOT)]⁺, [Rh(COD)]⁺, and [Rh(CO)Cl]-catalyzed (5 + 2) cycloadditions of VCP **1b** and phenylacetylene **2d**.

regioselectivity is similar to the [Rh(CO)Cl]-catalyzed reactions, while [Rh(dnCOT)]⁺ leads to higher regioselectivity, forming the distal products exclusively. These results are quite unintuitive, since the steric control of the aryl substituents should prefer the proximal products or lead to moderate selectivities, as in the reactions of TMS acetylene or 1-pentyne. After careful examination of the transition state geometries, it was found that the preference for the distal pathway with [Rh(dnCOT)]⁺ and [Rh(COD)]⁺ catalysts is due to the π/π and C-H/ π dispersion interactions between the aryl substituents and the ligand in the alkyne insertion transition state, as shown in Figure 6.

In the [Rh(dnCOT)]⁺-catalyzed distal transition state, *distal-TS2d-I*, the phenyl on the alkyne is positioned parallel with the naphthyl group on the dnCOT ligand. The distance between the center of the phenyl ring and the center of one of the rings in naphthyl is 4.12 Å, where stabilizing π/π interactions are expected.^{48,49} Previous benchmark calculations of the sandwich configuration of the benzene dimer showed that B3LYP predicts repulsive interactions at the aryl-aryl distance of 4.1 Å, while high level CCSD(T) calculations predict stabilizing

interactions of c.a. 1.5 kcal/mol.⁵⁰ In our calculations, B3LYP also significantly underestimates the ligand-substrate π/π interactions and predicts higher activation energies for the distal pathway. Since the phenyl group on alkyne is positioned far away from the ligand in the proximal pathway, no π/π interactions are possible. Thus, B3LYP erroneously predicts that the distal transition states are disfavored by 1.0–1.5 kcal/mol in the reactions with aryl acetylenes (Table 3, entries 13, 16, and 18). The D3(BJ) corrections give correct treatment of the dispersion interactions and significantly lower the energies of the distal transition states. The B3LYP-D3(BJ) results suggest that the distal products are formed exclusively in [Rh(dnCOT)]⁺-catalyzed reactions with aryl acetylenes, in good agreement with experiment.

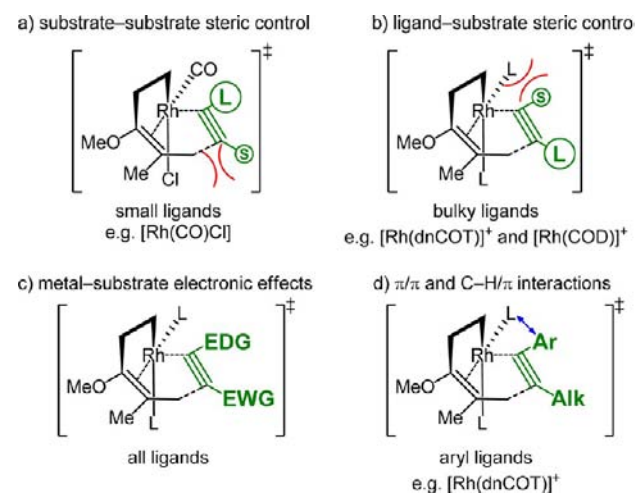
In the [Rh(COD)]⁺-catalyzed distal transition state, *distal-TS2d-II*, one of the C-H bonds on the COD ligand is positioned toward the center of the phenyl on the alkyne. The distance between the H atom and the center of the phenyl ring is 2.84 Å. Some stabilizing C-H/ π interactions are expected at this distance and orientation.^{50,51} Previous benchmark calculations of CH₄-benzene complexes showed that B3LYP

predicts repulsive interaction at this distance while CCSD(T) predicts a stabilizing interaction.^{44b} In our calculations, B3LYP also underestimates the ligand–substrate C–H/ π interactions in the distal transition state and erroneously predicts that the proximal product is favored. The D3(BJ) corrections again provide significant improvements to the B3LYP results and predict that the distal product is favored by a 10.6:1 ratio, in good agreement with experiment.

In summary, the regioselectivities of $[\text{Rh}(\text{dnCOT})]^+$ - and $[\text{Rh}(\text{COD})]^+$ -catalyzed reactions with aryl acetylenes are controlled by the ligand–substrate π/π and C–H/ π interactions. The stabilizing π/π and C–H/ π interactions reverse the steric effects and lead to the formation of distal products.

3.3. Summary of Effects of the Ligands and the Alkyne Substituents on Regioselectivities. In the above section, we have shown that the regioselectivity is dominated by different factors depending on the choice of the catalyst and the substrate. In this section, we summarize these factors and elucidate when a certain factor dominates regioselectivity (Scheme 2). These insights are essential to establish a predictive model for regioselectivities with different ligands and alkynes with different electronic and steric properties.

Scheme 2. Summary of Factors that Control Regioselectivities in Rh(I)-Catalyzed (5 + 2) Cycloadditions of Vinylcyclopropanes and Alkynes



3.3.1. Steric Effects. Two possible steric interactions might arise in the regioselectivity-determining alkyne insertion transition state: substrate–substrate repulsions between the alkyne substituent and the VCP terminus around the forming C–C bond, and ligand–substrate repulsions between the alkyne substituent and the ligand (a and b in Scheme 2, respectively). For reactions with sterically hindered alkyl and TMS substituted alkynes, the regioselectivity is dominated by steric effects. When small ligands are employed, such as in the $[\text{Rh}(\text{CO})\text{Cl}]$ catalyst, the substrate–substrate repulsions control the regioselectivity and lead to bond formation distal to the alkyne substituent. When larger ligands are employed, greater ligand–substrate repulsions are observed, leading to greater preference for the proximal products. When the alkyne substituent is a small alkyl group, e.g. for 1-pentyne ($R = n\text{-Pr}$), the regioselectivity is diminished.

3.3.2. Electronic Effects. The electron-withdrawing groups on the alkyne prefer to be proximal to the forming C–C bond to maximize the $d \rightarrow \pi^*$ backbonding interactions between the metal and the alkyne (Scheme 2c). Although less significant than the steric effects described above, these electronic effects become dominating and lead to enhanced or even reversed regioselectivities when the steric repulsions in the distal and proximal positions are comparable. These electronic effects will enhance the steric control in $[\text{Rh}(\text{dnCOT})]^+$ - and $[\text{Rh}(\text{COD})]^+$ -catalyzed reactions to increase the regioselectivity of proximal products and reverse the steric control in $[\text{Rh}(\text{CO})\text{Cl}]$ -catalyzed reactions to favor the formation of proximal products. On the contrary, electron-donating groups prefer to be distal to the forming C–C bond.

3.3.3. π/π and C–H/ π Interactions. The dnCOT ligand exhibits strong directing effects on the regioselectivities of aryl acetylenes via π/π dispersion interactions (Scheme 2d). The conformation of the naphthyl rings on the dnCOT ligand is more rigid than that in typical aryl phosphines. In the distal alkyne insertion transition states of $[\text{Rh}(\text{dnCOT})]^+$ -catalyzed reactions, the naphthyl ring parallels with the aryl group on the alkyne. These stabilizing π/π dispersion interactions dominate the regioselectivity and place these aryl groups distal to the forming C–C bond. The $[\text{Rh}(\text{COD})]^+$ catalyst has weaker C–H/ π dispersion interactions with aryl acetylenes and yields moderate regioselectivities.

4. CONCLUSIONS

We have investigated the mechanisms and origins of reactivities and regioselectivities of $[\text{Rh}(\text{dnCOT})]^+$ -, $[\text{Rh}(\text{COD})]^+$ -, and $[\text{Rh}(\text{CO})\text{Cl}]$ -catalyzed (5 + 2) cycloadditions of VCPs and alkynes. Although unique reactivities and regioselectivities have been observed experimentally for the $[\text{Rh}(\text{dnCOT})]^+$ and $[\text{Rh}(\text{COD})]^+$ catalysts, the mechanism and rate-determining step of the reactions with these catalysts are the same as in the $[\text{Rh}(\text{CO})\text{Cl}]$ -catalyzed reactions. The catalytic cycle involves cyclopropane ring-opening, alkyne insertion, reductive elimination, and ligand exchange. The rate- and regioselectivity controlling step is alkyne insertion and the catalyst resting state is the Rh-product complex.

The computations revealed the unique steric and dispersion effects of the dnCOT ligand on reactivity and regioselectivity. DFT calculations predicted higher reactivities of $[\text{Rh}(\text{dnCOT})]^+$ and $[\text{Rh}(\text{COD})]^+$ catalysts than of the $[\text{Rh}(\text{CO})\text{Cl}]$ catalyst in (5 + 2) cycloadditions, in good agreement with experiment. The high reactivities of these novel catalysts are due to the greater steric repulsions between the bulky ligand and the product in the Rh-product complex, which is the resting state in the catalytic cycle. In contrast, the rate-determining alkyne insertion transition state is not as sensitive to these steric effects. Thus, bulkier ligands lead to lower overall activation barriers and greater reactivities.

Substrate–substrate and ligand–substrate steric repulsions, electronic effects, and ligand–substrate π/π and C–H/ π interactions can all contribute to the regiochemical control of the reactions with different catalysts and alkynes. Careful examinations of these factors indicated that high regioselectivities to form both distal and proximal products can be achieved with various alkynes by a proper choice of ligand. We established the scenarios in which certain factors dominate over other effects and control the regioselectivity (Scheme 2). When alkyl and TMS substituted alkynes are used, the regioselectivity is determined by steric effects. Smaller ligands

prefer distal products and bulkier ligands prefer proximal products. Electronic effects become dominant when the alkyne substituent is small and strongly electron-withdrawing, such as formyl or acyl. Strongly electron-withdrawing alkyne substituents prefer the proximal pathway, and enhance the proximal steric control by bulky ligands, or reverse the distal steric control when small ligands are used. Aryl substituents on the alkynes show strong directing effects to favor the distal products when $[\text{Rh}(\text{dnCOT})]^+$ or $[\text{Rh}(\text{COD})]^+$ catalysts are used. This is due to stabilizing ligand–substrate π/π and C–H/ π interactions between the ligand and the aryl substituent on the alkyne in the distal pathway. Understanding these steric, electronic, and noncovalent dispersion effects of the ligands and the alkyne substituents can help design new catalysts for highly selective cycloaddition reactions.

■ ASSOCIATED CONTENT

Supporting Information

Complete ref 29 and optimized geometries and energies of all computed species. This material is available free of charge via the Internet at <http://pubs.acs.org>.

■ AUTHOR INFORMATION

Corresponding Author

houk@chem.ucla.edu (K.N.H.); wenderp@stanford.edu (P.A.W.)

Notes

The authors declare no competing financial interest.

■ ACKNOWLEDGMENTS

We are grateful to the National Science Foundation (K.N.H., CHE-1059084; P.A.W., CHE-0450638) and the Natural Science Foundation of China (X.F.X., 21103094) for financial support of this research. Calculations were performed on the Hoffman2 cluster at UCLA and the Extreme Science and Engineering Discovery Environment (XSEDE), which is supported by the NSF.

■ REFERENCES

- (1) Wender, P. A.; Croatt, M. P.; Deschamps, N. M. In *Comprehensive Organometallic Chemistry III*; Ojima, I., Ed.; Elsevier Ltd.: Amsterdam, 2007; Vol 10, pp 603–648.
- (2) Wender, P. A.; Takahashi, H.; Witulski, B. *J. Am. Chem. Soc.* **1995**, *117*, 4720–4721.
- (3) For intermolecular reactions involving alkynes: (a) Wender, P. A.; Rieck, H.; Fujii, M. *J. Am. Chem. Soc.* **1998**, *120*, 10976–10977. (b) Wender, P. A.; Dyckman, A. J.; Husfeld, C. O.; Scanio, M. J. *C. Org. Lett.* **2000**, *2*, 1609–1611. (c) Wender, P. A.; Barzilay, C. M.; Dyckman, A. J. *J. Am. Chem. Soc.* **2001**, *123*, 179–180. (d) Wender, P. A.; Gamber, G. G.; Scanio, M. J. *C. Angew. Chem., Int. Ed.* **2001**, *40*, 3895–3897. (e) Liu, P.; Sirois, L. E.; Cheong, P. H. Y.; Yu, Z. X.; Hartung, I. V.; Rieck, H.; Wender, P. A.; Houk, K. N. *J. Am. Chem. Soc.* **2010**, *132*, 10127–10135. (f) Wender, P. A.; Stemmler, R. T.; Sirois, L. E. *J. Am. Chem. Soc.* **2010**, *132*, 2532–2533.
- (4) For intermolecular reactions involving allenes: Wegner, H. A.; de Meijere, A.; Wender, P. A. *J. Am. Chem. Soc.* **2005**, *127*, 6530–6531.
- (5) For recent reviews of transition-metal catalyzed (5 + 2) cycloadditions: (a) Wender, P. A.; Gamber, G. G.; Williams, T. J. in: *Modern Rhodium-Catalyzed Organic Reactions*, (Ed.: Evans, P. A.), Wiley-VCH, Weinheim, 2005, pp 263–299. (b) Wender, P. A.; Croatt, M. P.; Deschamps, N. M. in: *Comprehensive Organometallic Chemistry III*; Crabtree, R. H., Mingos, D. M. P., Eds.; Elsevier: Oxford, 2007; Vol. 10, pp 603–647. (c) Butenschön, H. *Angew. Chem., Int. Ed.* **2008**,

47, 5287–5290. (d) Pellissier, H. *Adv. Synth. Catal.* **2011**, *353*, 189–218.

(6) For Ru, Ni, and Fe-catalyzed (5 + 2) cycloadditions, see: (a) Trost, B. M.; Toste, F. D.; Shen, H. *J. Am. Chem. Soc.* **2000**, *122*, 2379. (b) Trost, B. M.; Shen, H. *C. Angew. Chem., Int. Ed.* **2001**, *40*, 2313. (c) Trost, B. M.; Shen, H. C.; Horne, D. B.; Toste, E. D.; Steinmetz, B. G.; Koradin, C. *Chem.—Eur. J.* **2005**, *11*, 2577–2590. (d) Zuo, G.; Louie, J. *J. Am. Chem. Soc.* **2005**, *127*, 5798–5799. (e) Fürstner, A.; Majima, K.; Martin, R.; Krause, H.; Kattinig, E.; Goddard, R.; Lehmann, C. W. *J. Am. Chem. Soc.* **2008**, *130*, 1992–2004.

(7) Wang, B.; Cao, P.; Zhang, X. M. *Tetrahedron Lett.* **2000**, *41*, 8041–8044.

(8) Wender, P. A.; Williams, T. J. *Angew. Chem., Int. Ed.* **2002**, *41*, 4550–4553.

(9) (a) Wender, P. A.; Sirois, L. E.; Stemmler, R. T.; Williams, T. J. *Org. Lett.* **2010**, *12*, 1604–1607. (b) Wender, P. A.; Lesser, A. B.; Sirois, L. E. *Org. Synth.* **2011**, *88*, 109–120.

(10) (a) Lee, S. I.; Park, Y.; Park, J. H.; Jung, G.; Choi, S. Y.; Chung, Y. K.; Lee, B. Y. *J. Org. Chem.* **2006**, *71*, 91–96. (b) Gomez, F. J.; Kamber, N. E.; Deschamps, N. M.; Cole, A. P.; Wender, P. A.; Waymouth, R. M. *Organometallics* **2007**, *26*, 4541–4545.

(11) Saito, A.; Ono, T.; Hanzawa, Y. *J. Org. Chem.* **2006**, *71*, 6437–6443.

(12) Wender, P. A.; Love, J. A.; Williams, T. J. *Synlett* **2003**, 1295–1298.

(13) Wender, P. A.; Haustedt, L. O.; Lim, J.; Love, J. A.; Williams, T. J.; Yoon, J.-Y. *J. Am. Chem. Soc.* **2006**, *128*, 6302–6303.

(14) Shintani, R.; Nakatsu, H.; Takatsu, K.; Hayashi, T. *Chem.—Eur. J.* **2009**, *15*, 8692–8694.

(15) (a) Wender, P. A.; Gamber, G. G.; Hubbard, R. D.; Zhang, L. *J. Am. Chem. Soc.* **2002**, *124*, 2876–2877. (b) Wang, Y.; Wang, J.; Su, J.; Huang, F.; Jiao, L.; Liang, Y.; Yang, D.; Zhang, S.; Wender, P. A.; Yu, Z.-X. *J. Am. Chem. Soc.* **2007**, *129*, 10060–10061. (c) Huang, F.; Yao, Z.-K.; Wang, Y.; Wang, Y.; Zhang, J.; Yu, Z.-X. *Chem. Asian J.* **2010**, *5*, 1555–1559.

(16) Wender, P. A.; Gamber, G. G.; Hubbard, R. D.; Pham, S. M.; Zhang, L. *J. Am. Chem. Soc.* **2005**, *127*, 2836–2837.

(17) (a) Jiao, L.; Ye, S. Y.; Yu, Z.-X. *J. Am. Chem. Soc.* **2008**, *130*, 7178–7179. (b) Jiao, L.; Lin, M.; Yu, Z.-X. *Chem. Commun.* **2010**, *46*, 1059–1061.

(18) Jiang, G.-J.; Fu, X.-F.; Li, Q.; Yu, Z.-X. *Org. Lett.* **2012**, *14*, 692–695.

(19) Inagaki, F.; Sugikubo, K.; Miyashita, Y.; Mukai, C. *Angew. Chem., Int. Ed.* **2010**, *49*, 2206–2210.

(20) Wender, P. A.; Correa, A. G.; Sato, Y.; Sun, R. *J. Am. Chem. Soc.* **2000**, *122*, 7815–7816.

(21) For representative synthetic applications, see: (a) Wender, P. A.; Fujii, M.; Husfeld, C. O.; Love, J. A. *Org. Lett.* **1999**, *1*, 137–139. (b) Wender, P. A.; Zhang, L. *Org. Lett.* **2000**, *2*, 2323–2326. (c) Wender, P. A.; Bi, F. C.; Brodney, M. A.; Gosselin, F. *Org. Lett.* **2001**, *3*, 2105–2108. (d) Ashfeld, B. L.; Martin, S. F. *Org. Lett.* **2005**, *7*, 4535–4537. (e) Ashfeld, B. L.; Martin, S. F. *Tetrahedron* **2006**, *62*, 10497–10506. (f) Trost, B. M.; Hu, Y.; Horne, D. B. *J. Am. Chem. Soc.* **2007**, *129*, 11781–11790. (g) Trost, B. M.; Waser, J.; Meyer, A. *J. Am. Chem. Soc.* **2008**, *130*, 16424–16434.

(22) For an alternative approach to rhodacycles for (5 + 2) cycloadditions, see: (a) Shu, X.-Z.; Huang, S.; Shu, D.; Guzei, I. A.; Tang, W. *Angew. Chem., Int. Ed.* **2011**, *50*, 8153–8156. (b) Shu, X.-Z.; Li, X.; Shu, D.; Huang, S.; Schienebeck, C. M.; Zhou, X.; Robichaux, P. J.; Tang, W. *J. Am. Chem. Soc.* **2012**, *134*, 5211–5221.

(23) Wender, P. A.; Lesser, A. B.; Sirois, L. E. *Angew. Chem., Int. Ed.* **2012**, *51*, 2736–2740.

(24) (a) Yu, Z.-X.; Wender, P. A.; Houk, K. N. *J. Am. Chem. Soc.* **2004**, *126*, 9154–9155. (b) Yu, Z.-X.; Cheong, P. H.-Y.; Liu, P.; Legault, C. Y.; Wender, P. A.; Houk, K. N. *J. Am. Chem. Soc.* **2008**, *130*, 2378–2379. (c) Liu, P.; Cheong, P. H.-Y.; Yu, Z.-X.; Wender, P. A.; Houk, K. N. *Angew. Chem., Int. Ed.* **2008**, *47*, 3939–3941.

- (25) (a) For a theoretical study of $[\text{Rh}(\text{dppp})]\text{SbF}_6$ -catalyzed (3 + 2) cycloaddition of VCPs and alkynes and alkenes: Jiao, L.; Lin, M.; Yu, Z.-X. *J. Am. Chem. Soc.* **2011**, *133*, 447–461. (b) For a theoretical study of $[\text{Rh}(\text{CO})_2\text{Cl}]_2$ -catalyzed (5 + 2) cycloaddition of cyclopropylimines and alkynes: Montero-Campillo, M. M.; Cabaleiro-Lago, E. M.; Rodriguez-Otero, J. *J. Phys. Chem. A* **2008**, *112*, 9068–9074.
- (26) For a review of theoretical studies of regioselectivities in C–C bond-forming reactions with alkynes: Liu, P.; Houk, K. N. *Inorg. Chim. Acta* **2011**, *369*, 2–14.
- (27) (a) Wender, P. A.; Christy, J. P. *J. Am. Chem. Soc.* **2007**, *129*, 13402–13403. (b) Wender, P. A.; Christy, J. P.; Lesser, A. B.; Gieseler, M. T. *Angew. Chem., Int. Ed.* **2009**, *48*, 7687–7690.
- (28) (a) Becke, A. D. *J. Chem. Phys.* **1993**, *98*, 5648. (b) Lee, C.; Yang, W.; Parr, R. G. *Phys. Rev. B* **1988**, *37*, 785.
- (29) Frisch, M. J. et al. *Gaussian 03*, Rev. E.01; Gaussian, Inc.: Wallingford CT, 2004.
- (30) Andrae, D.; Haussermann, U.; Dolg, M.; Stoll, H.; Preuss, H. *Theor. Chim. Acta* **1990**, *77*, 123–141.
- (31) (a) Barone, V.; Cossi, M. *J. Phys. Chem. A* **1998**, *102*, 1995–2001. (b) Cossi, M.; Rega, N.; Scalmani, G.; Barone, V. *J. Comput. Chem.* **2003**, *24*, 669–681.
- (32) Grimme, S. *DFTD3*, V2.0 Rev 1; University Münster: Münster, Germany, 2010.
- (33) Grimme, S.; Antony, J.; Ehrlich, S.; Krieg, H. *J. Chem. Phys.* **2010**, *132*, 154104.
- (34) Grimme, S.; Ehrlich, S.; Goerigk, L. *J. Comput. Chem.* **2011**, *32*, 1456–1465.
- (35) Grimme, S. *J. Comput. Chem.* **2006**, *27*, 1787–1799.
- (36) Legault, C. Y. *CYLview*, 1.0b; Université de Sherbrooke: Sherbrooke, Québec, Canada, 2009 (<http://www.cylview.org>).
- (37) See SI for more details.
- (38) For effects of counterions in (5 + 2) cycloadditions with cationic rhodium(I) catalysts, see: refs 8, 9a.
- (39) We also computed the alternative catalytic cycle employing the diene product as ligand in place of dnCOT or COD. This process is highly unfavorable, with an overall free energy span of 37.8 kcal/mol with diene product *proximal-3a* as ligand when dnCOT is also present in the system. See SI for more details of these calculations.
- (40) In the reaction with $[\text{Rh}(\text{dnCOT})]^+$, the Rh-product complex (*proximal-cpx5a-I*) and the Rh-allyl complex (*cpx2-I*) have essentially the same energies (–5.9 and –6.0 kcal/mol, respectively). We used the Rh-product complex (*proximal-cpx5a-I*) as the resting state in the calculations to simplify the discussion and comparisons with other catalysts.
- (41) Kozuch, S.; Shaik, S. *Acc. Chem. Res.* **2011**, *44*, 101–110.
- (42) The free energy span model was also employed in our previous theoretical study on the reactivity of VCPs in (5 + 2) cycloadditions. See ref. 24c.
- (43) In the reaction with $[\text{Rh}(\text{CO})\text{Cl}]$ catalyst, the proximal pathway is disfavored by 2.2 kcal/mol (Table 2, entry 3). This suggests the distal product is the major product, while the proximal pathway is competing. The two product complexes are likely to be in rapid equilibrium via ligand exchange. Considering the Rh catalyst is only substoichiometric, most of the catalyst is likely to form the more stable complex with the proximal product.
- (44) (a) Zhao, Y.; Truhlar, D. G. *Phys. Chem. Chem. Phys.* **2005**, *7*, 2701–2705. (b) Zhao, Y.; Truhlar, D. G. *J. Chem. Theory Comput.* **2007**, *3*, 289–300.
- (45) For a recent review: Grimme, S. *WIREs Comput. Mol. Sci.* **2011**, *1*, 211–228.
- (46) (a) Zhao, Y.; Truhlar, D. G. *Theor. Chem. Acc.* **2008**, *120*, 215. (b) Zhao, Y.; Truhlar, D. G. *Acc. Chem. Res.* **2008**, *41*, 157.
- (47) Ethynamine was used in the calculations as a model electron-rich alkyne. Experiments have not been performed on ethynamine. Such alkynes are typically highly reactive and prone to decomposition.
- (48) (a) Sinnokrot, M. O.; Valeev, E. F.; Sherrill, C. D. *J. Am. Chem. Soc.* **2002**, *124*, 10887–10893. (b) Sinnokrot, M. O.; Sherrill, C. D. *J. Phys. Chem. A* **2004**, *108*, 10200–10207. (c) Sinnokrot, M. O.; Sherrill, C. D. *J. Phys. Chem. A* **2006**, *110*, 10656–10668.
- (49) Fan, Y.-B.; Tao, F.-G.; Xu, W.; Hua, Z.-Y. *Acta Chim. Sin.* **1999**, *57*, 1–4.
- (50) Takatani, T.; Sherrill, C. D. *Phys. Chem. Chem. Phys.* **2007**, *9*, 6106–6114.
- (51) This distance is comparable to the H–aryl distance at the distal transition state for the reaction with TMS acetylene and $[\text{Rh}(\text{dnCOT})]^+$ catalyst (2.77 Å in *distal-TS2a-I*). See Figure 2.